

MR-Compatible of a SiPM-Based PET Detector Module Using HDMI for Analog Readout and Power Supply

Jonathan D. Thiessen¹, Eric Berg², Chen-Yi Liu^{1,3}, Daryl Bishop⁴, Piotr Kozłowski^{5,6}, Fabrice Retière⁴, Vesna Sossi⁶, Greg Stortz⁶, Christopher J. Thompson⁷, Xue Zhu Zhang¹, and Andrew L. Goertzen^{1,3}

¹Radiology, University of Manitoba, Winnipeg, Manitoba, Canada, ²Biomedical Engineering, University of California, Davis, Davis, California, United States, ³Physics & Astronomy, University of Manitoba, Winnipeg, Manitoba, Canada, ⁴Detector Development Group, TRIUMF, Vancouver, British Columbia, Canada, ⁵Radiology, University of British Columbia, Vancouver, British Columbia, Canada, ⁶Physics & Astronomy, University of British Columbia, Vancouver, British Columbia, Canada, ⁷McConnell Brain Imaging Centre, Montreal Neurological Institute, Montreal, Quebec, Canada

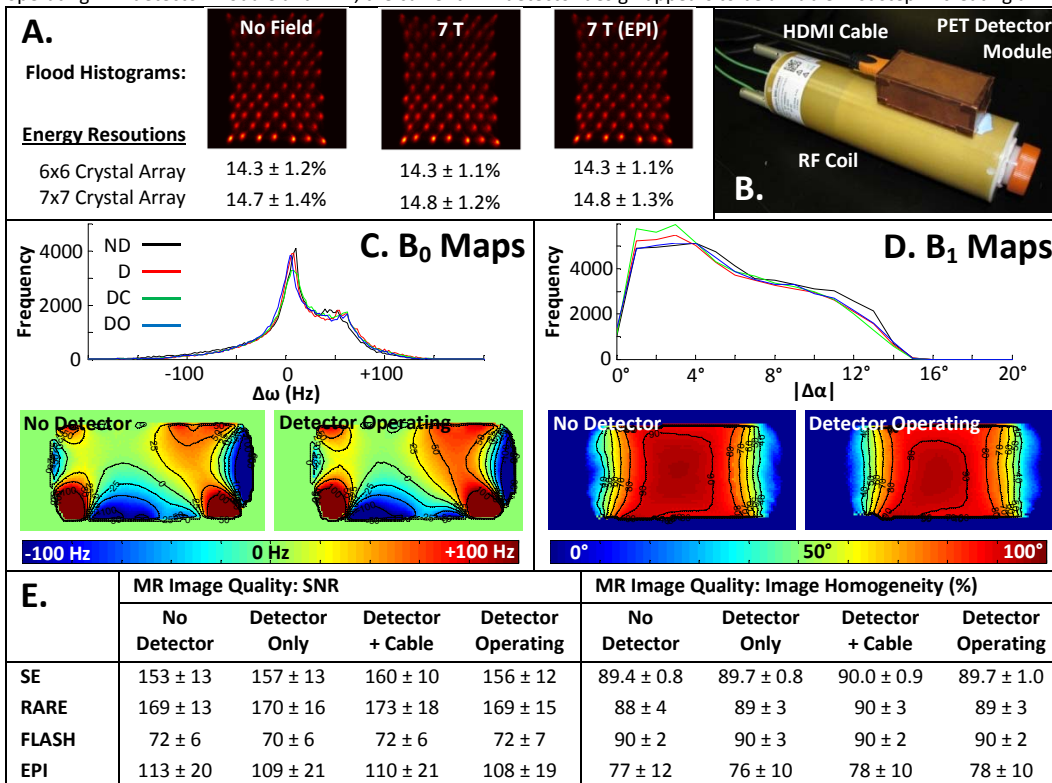
Purpose Positron emission tomography (PET) reveals dynamic and molecular level processes through the use of radioactively labeled pharmaceuticals. PET/MRI systems benefit from the complementary molecular level functional images of PET and the anatomical and functional images of MRI. Pre-clinical MR-compatible PET systems have been demonstrated using avalanche photodiodes (APDs)¹⁻⁴ and more recently, Geiger-mode APDs (also known as silicon photomultipliers, or SiPMs) with performance characteristics superior to APDs⁵⁻⁸. An MR-compatible SiPM PET detector module with a dual-layer LYSO scintillator crystal array using a High-Definition Multimedia Interface (HDMI) cable for supplying power and bias as well as transmitting analog signals was tested in a 7 T Bruker MRI. Performance of the PET detector was evaluated inside the MRI as was performance of the MRI with the PET detector present and operating. This work represents initial efforts in creating a full-ring MR-compatible PET system featuring 16 individual PET detector modules.

Methods *PET Detector Module with HDMI Readout:* Detector module consists of a SensL SPMArray4 photodetector with a dual-layer LYSO crystal array with 7x7 crystals in the bottom layer and 6x6 crystals offset in the top layer. Analog signals from the SiPM are multiplexed from 16 to 4 signals with a resistor network. It is housed in a light-tight box constructed of double-sided copper-clad printed circuit board (each copper layer is ~35 μm thick). An 8 m long HDMI cable consisting of 4 pairs of shielded 100 Ω differential lines plus 7 individual lines connects to a receiver card that provides power (30 V bias and ±5 V for pre-amplifiers) and has 4 50 Ω single-ended outputs. Timing and shaping of the signals was accomplished with a series of NIM electronics and a PC-based ADC card. Flood histograms and energy resolution were calculated for each crystal in the array. *MRI:* An H₂O phantom containing 1 g/l Cu₂SO₄•5H₂O and 3.6 g/l NaCl was imaged using a quadrature volume RF coil with a 35 mm inner diameter (Bruker, Germany) in a 7 T Bruker Avance III MRI system. A series of 3D FLASH images were acquired for B₀ field maps (T_E = 1.71 and 5.71 ms, T_R = 20 ms) and B₁ field maps⁹ (α = 145°, 180°, and 215°, T_E = 6 ms, T_R = 33 ms) with a 3.5x3.5x7 cm FOV and 64x64x128 matrix size encompassing the volume of the phantom visible in the RF coil. To evaluate MR image quality, 11 slices were placed (1 mm slice thickness, 3 mm inter-slice distance) along the extent of the phantom with an in-plane FOV of 3.5x3.5 cm and 128x128 matrix. Spin echo (T_E = 56 ms, T_R = 1500 ms), RARE (effective T_E = 56 ms, T_R = 1500 ms, RARE factor = 8), FLASH (α = 20°, T_E = 6 ms, T_R = 150 ms), and single-shot echo planar (T_E = 50 ms, T_R = 3 s, 64x64 matrix) images were acquired with 1 average and 5 repetitions each.

PET/MRI: To evaluate the influence of the detector and cabling on the MRI, sequences were repeated with 4 different detector module configurations: no detector (ND), with the detector placed directly above the RF coil (D), with the HDMI cable attached to the detector (DC), and during acquisition of flood histograms (DO). A ²²Na source was attached to the RF coil immediately in front of the detector module for all acquisitions. The influence of the orientation and configuration of the PET detector on the field intensity of the RF coil was measured with a network analyzer. B₀ and B₁ field maps, SNR, and image homogeneity were calculated in MATLAB based on regions of interest defined using a threshold mask.

Results and Discussion *PET Detector in MRI:* There was no difference in the energy resolution of the flood histogram data acquired outside the magnet and inside the magnet during various pulse sequences (Fig. A). When inside the MRI, there was a noticeable increase in the photopeak amplitude (e.g. 4.3±0.2 V outside the magnet vs. 4.6±0.3 V inside the magnet). This was attributed to a decrease in the detector temperature, which was not monitored or corrected for. *MRI with PET Detector:* The B₁ field intensity was unchanged with the detector operating adjacent to the RF coil, although if placed in the opposite direction, such that the detector hung over the end of the coil, field intensity decreased by ~0.1 dB, suggesting that coupling of the RF coil with the copper shielding and cabling of the PET detector is dependent on orientation. A cable trap on the HDMI cable had no effect on B₁ field intensity, however there was a small decrease (< 0.1 dB) when the HDMI cable was adjacent to the RF coil cable. The operating detector did not have a significant impact on B₀ and B₁ homogeneity, SNR, and image homogeneity (Fig. C-E).

Conclusion HDMI is a low cost cabling solution with a robust connector, 100 Ω differential signalling, and high bandwidth. Given the limited interactions between the operating PET detector module and MRI, the current PET detector design appears to be a viable first step in creating an MR-compatible full-ring PET system.



Figures A. Flood histograms and energy resolutions of PET detector operating inside/outside the MRI. **B.** PET detector module with HDMI cable on top of the RF coil. **C.** Histogram of values in the B₀ field deviating from the Larmor frequency, Δω₀ (Hz), with cross-sections of the B₀ maps. **D.** Histogram of the absolute values in the B₁ field deviating from a 90° pulse, |Δα|, with cross-sections of the B₁ maps. **E.** Mean ± σ of SNR and image homogeneity for images acquired with different pulse sequences and detector configurations.

References 1. Pichler et al., J Nucl Med 47:639-47 (2006) 2. Catana et al., PNAS 105:3705-10 (2008) 3. Judenhofer et al., Nature Med 14:459-65 (2008) 4. Wehrl et al., MRM 65:269-79 (2011) 5. Hong et al., IEEE TNS 55:882-88 (2008) 6. Yamamoto et al., Phys Med Biol 55:5817-31 7. Kolb et al., Phys Med Biol 55:1815-32 8. Maramraju et al., IEEE TNS 59:1892-99 (2012) 9. Dowell and Tofts, MRM 58:622-630

Acknowledgments Funding provided by NSERC and Manitoba Health Research Council. Thanks to Scott King for network analysis of the RF coil.